*Journal of Alloys and Compounds, 189* (1992) 87–96
*JALCOM 355*



# Stable and metastable phases in the metal-rich Y–Zr–Si system and their hydrogen reactivity

V. Kotroczo, I. J. McColm, M. Rebbeck and J. M. Ward
*Department of Industrial Technology, University of Bradford, Bradford BD7 1DP (UK)*

(Received January 29, 1992; in final form April 17, 1992)

**Abstract**

Rapid cooling of small samples from the series $Y_5Si_3$–$Zr_5Si_3$ has enabled a complete range of hexagonal $D8_8$ phases to be made. The hydrogen reactivity of these metastable phases shows that increasing zirconium in $Y_{5-x}Zr_xSi_3$ decreases the stability of the hydrides formed. Beyond the composition $Y_{4.25}Zr_{0.75}Si_3$, the ability of the phase to desorb rapidly about 0.9H $mol^{-1}$ is lost. $Zr_5Si_3$ is shown to be stable only when quenched from the melt, while $Zr_5Ge_3$ anneals to a well-defined $D8_8$ phase. A 1250 °C annealing programme carried out on metal-rich arc casts has enabled a section of the Y–Zr–Si phase diagram to be presented. Limiting compositions in the annealed samples are $Y_{4.78}Zr_{0.23}Si_3$, $Zr_{4.55}Y_{0.45}Si_3$, $Zr_{4.0}Y_{1.1}Si_3$ and $Zr_{1.83}Y_{0.21}Si$. The hydrogen reactivity and X-ray parameters of these phases are reported.

## 1. Introduction

The $D8_8$ special ceramic silicide $Y_5Si_3$, possessing elements of covalent bonding, has been examined [1–3] as a hydrogen storage system which might overcome the decrepitation problem $LaNi_5$ experiences on repeated absorption and desorption cycles. However, the temperature needed to desorb hydrogen at 1 atm pressure from $Y_5Si_3H_{2.5}$ is high, in the region of 485 °C. Using the enthalpy of formation of the binary hydrides as a guide (Table 1), it was thought that substitution of scandium for yttrium might lower the desorption temperature and this was found to be the case [6]. The data in Table 1 suggest from a simple enthalpy argument that zirconium might be more effective in lowering the desorption temperature. A phase $Zr_5Si_3$ stabilized by small amounts of non-metal is reported to have the $D8_8$ structure [7], but its reported lattice parameters, $a = 0.797$ nm and $c = 0.557$ nm, dictate a unit cell volume well outside a 15% difference compared with $Y_5Si_3$, which leads in turn to an expectation of a very limited range of solid solubility between $Zr_5Si_3$ and $Y_5Si_3$. The partially covalent nature of the bonding in these systems does frequently lead to metastable phase formation on fast cooling of small samples from the melt and hence it was felt that significant amounts of zirconium may be substituted for yttrium in $Y_5Si_3$ such that the effect of zirconium on the hydrogen reactivity of $Y_5Si_3$ may be determined. This paper reports on the existence of a range of metastable solid solutions as determined by X-ray, microscopic and energy-dispersive X-ray (EDX) analysis of surfaces prepared for scanning electron microscopic examination and by the hydrogen reactivity of the specimens. Annealing the cast specimens at 1050 and 1250 °C does produce the equilibrium phase assemblages which enable the solubilities of zirconium in $Y_5Si_3$ and yttrium in $Zr_5Si_3$ and $Zr_2Si$ to be determined. Metastable and stable products from several Y–Zr–Si preparations from the molten state have been established and their hydrogen reactivity determined.

TABLE 1. Hydrogen affinities of some $D8_8$-forming elements

| Element | Hydride | $\Delta H_f^\circ$ (kJ $mol^{-1}$) | Reference |
|---|---|---|---|
| Y | $YH_2$ | −226.0 | [4] |
| Zr | $ZrH_2$ | −160.4 | [4] |
| Sc | $ScH_2$ | −200.6 | [5] |
| Si | $SiH_4$ | 34.3 | [4] |
| Ge | $GeH_4$ | 90.4 | [4] |

The region investigated was the metal-rich system with silicon in the 22–37.5 at.% range, with emphasis on the $Y_5Si_3$–$Zr_5Si_3$ solid solution region. Three samples containing germanium and scandium have also been prepared and are reported by way of comparison.

In the region chosen for study there is a notable difference in the two basic systems. $Y_5Si_3$ is the only silicide phase up to 37.5 at.%; it is easily prepared by arc melting and shows no stoichiometric variation on

0925-8388/92/$5.00

the metal-rich side of the stoichiometric composition [8]. In the Zr–Si system a metal-rich phase exists with a tetragonal symmetry and lattice parameters $a = 0.6612$ nm and $c = 0.5294$ nm, but some doubt exists as to its composition, with $Zr_2Si$ and $Zr_4Si$ both being reported [9, 10]. The most recent phase diagram compilation by Massalski [11] shows that in the zirconium-rich region $\alpha$- and $\beta$-ZrSi have been reported together with $\beta$-$Zr_5Si_4$, $Zr_3Si_2$ and $Zr_5Si_3$, existing only as a high temperature phase, $Zr_2Si$ and possibly $Zr_3Si$. The $D8_8$ phase $Zr_5Si_3$ is not so readily made by arc melting and it is suggested that its existence is dependent on the presence of oxygen impurities in the octahedral sites formed from six zirconium atoms. Unstated oxygen compositions in the octahedral sites have led to some discrepancies in the reported lattice parameters and, arguing by analogy with the $Y_5Si_3$ system [8], the less oxygen it contains, the larger the unit cell volume is expected to be, since both the $a$ and $c$ axes are extended when there are fewer electrons donated from the octahedral sites. The data presented here support the view that it is not a stable phase in the Zr–Si system but can be prepared by rapid cooling from the melt.

## 2. Experimental details

The techniques used throughout this work have been fully described in several previous papers [1, 6, 8], but two areas need to be re-emphasized since the results obtained are dependent on them. The first is the nature of the preparative method which produces small samples in the range of 0.5 g in a furnace operating at a pressure above 1 atm of argon with the purified gas sweeping through the very small reaction chamber. This leads to high purity since surface contaminants are swept away, but, more importantly in this work, it produces rapid cooling from the liquid state when the arc current is switched off. Typical cooling curves are shown in Fig. 1; these show 700–900 °C cooling over a 5 s period, which can be sufficient to freeze in metastable phases in systems. Sample surface temperatures were measured by collecting radiant energy in an IRCON model 11×30 pyrometer assuming black-body radiation and focusing the optical system on 1 $mm^2$ surface.

When samples were annealed, they were wrapped in tantalum foil and encapsulated in silica tubes which were first evacuated and then partially filled with high purity argon gas. Only metals of high purity, 99.99%, as supplied by Rare Earth Products and silicon of 99.999% purity from Koch–Light were used in the form of cut pieces, not as powders, in order to limit impurity uptake.

Much of the phase analysis was done on a scanning electron microscope. An ISI Super IIIA scanning electron microscope (SEM) with a Link Systems 840A EDX analyser was used to determine the microstructure. Atomic number contrast from the backscatter detector distinguished the phases in polished, unetched specimens. The standards for the EDX analysis were prepared from polished pieces of the same high purity elements used for the preparation of the arc-melted samples.

## 3. Results and discussion

### 3.1. $Zr_5Si_3$, $Zr_5Ge_3$, $Y_5Si_3$

These three preparations produced the cooling curves shown in Fig. 1, two of which suggested non-equilibrium phase assemblages for $Zr_5Si_3$ and $Zr_5Ge_3$ from the sloping solidification plateau for $Zr_5Ge_3$ and the convex cooling curves for both $Zr_5Si_3$ and $Zr_5Ge_3$; such features are indicative of solid state reactions occurring on cooling. $Y_5Si_3$ produced simple cooling curves at all rates of cooling and the X-ray analysis showed only a single-phase hexagonal material with $a = 0.8442$ nm and $c = 0.6333$ nm. In contrast, $Zr_5Si_3$ produces quite a complex picture, each preparation from the arc furnace being multiphase, with the major component being a dark phase of about 90% on the SEM picture. The dark phase gave an analysis $Zr_{4.95}Si_3$ and a corresponding hexagonal $D8_8$ X-ray pattern with $a = 0.7959$ nm and $c = 0.5561$ nm. These lattice parameters are significantly larger than the literature values of $a = 0.7854$ nm and $c = 0.5535$ nm, suggesting that the phase prepared here contains less impurity non-metal such as oxygen in the octahedral $Zr_6$ sites. The EDX scan showed the light areas to be an 89at.%Zr–11at.%Si eutectic. Extra lines on the X-ray pattern confirmed the zirconium metal but also showed the presence of an orthorhombic phase with parameters $a = 0.697$ nm, $b = 0.379$ nm and $c = 0.530$ nm; these are close to a reported ZrSi orthorhombic phase. The purity, and hence metastability, of the $Zr_5Si_3$ was evident on annealing for 7 days at 1250 °C, when the hexagonal $D8_8$ phase in the X-ray pattern disappeared completely, being replaced by a strong pattern indexing as orthorhombic ZrSi plus some weak extra lines from the tetragonal $Zr_3Si$ phase. Thus in the absence of impurities, probably oxygen, $Zr_5Si_3$ can only be made by rapid cooling of the melt.

Since the original preparations contained more than 90% $Zr_5Si_3$ it was felt to be worthwhile testing the hydrogen reactivity at 1 atm $H_2$ up to 600 °C. There was a rapid reaction at 204 °C taking the overall composition to $Zr_5Si_3H_{0.54}$, which when examined showed this to be the result of transforming the Zr–Si eutectic to $ZrH_2$. It is worth noting the very low temperature at which this reaction proceeds compared with the reaction of bulk zirconium metal with hydrogen,

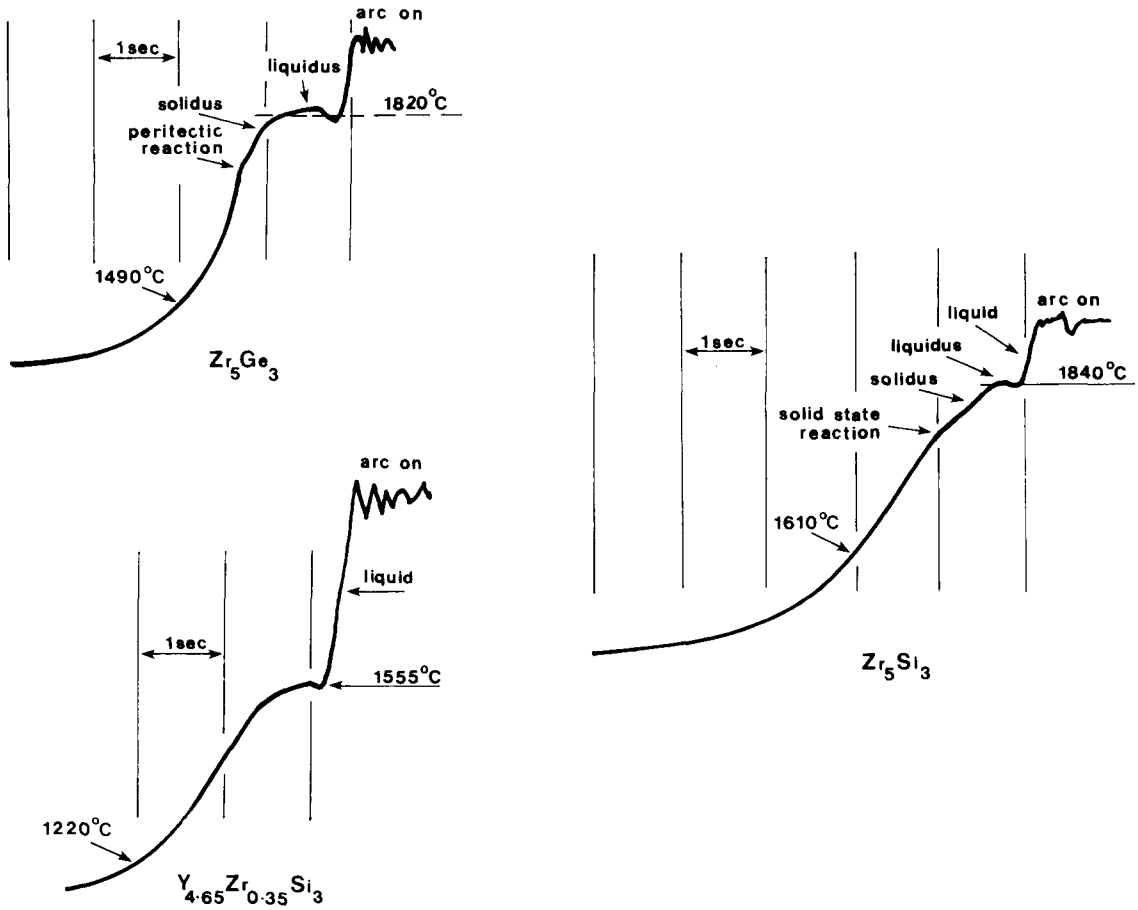


Fig. 1. Cooling curves for 0.5 g samples showing the rapid rate of cooling achieved in the furnace used and the appearance of curves suggesting various solid state reactions.

which begins at 415 °C and becomes rapid at 562 °C. After this rapid uptake there was a slow weight gain in the sample up to $Zr_5Si_3H_{1.62}$ on cooling from 600 °C to room temperature. Reheating leads to a temperature-dependent slow loss of 0.54H mol$^{-1}$ which is regained on cooling; this can be written as

$$Zr_5Si_3 + Zr\text{–}Si + H_2 \longrightarrow 0.27(Zr\text{–}Si)H_2 + 0.73Zr_5Si_3H_{1.48} \quad (1)$$

Taking eqn. (1) to summarize the reaction occurring, it appears that $Zr_5Si_3$ slowly absorbs about 1.5H mol$^{-1}$, with 0.5H mol$^{-1}$ able to be cycled at 1 atm $H_2$ pressure through a 575 °C temperature interval.

As in the $Zr_5Si_3$ case, the phase assemblage of arc-cast $Zr_5Ge_3$ was a complex, intimate mixture of light and dark phases on the SEM pictures. Spot analysis showed the light phase to vary in composition from $Zr_{2.90}Ge$ to $Zr_{2.79}Ge$, while the dark phase was an intimate mixture of ZrGe and $Zr_3Ge$ analysing overall to $Zr_{5.4}Ge_3$. This mixture produced a complex X-ray pattern which confirmed this interpretation. Exposure of the sample to hydrogen showed no reaction up to 600 °C, confirming the absence of zirconium eutectic and any $D8_8$ $Zr_5Ge_3$ phase. Now, in contrast to $Zr_5Si_3$ however, when the sample was annealed at 1250 °C for 7 days, a virtually single-phase material with the $D8_8$ structure and lattice parameters $a = 0.8053$ nm and $c = 0.5620$ nm emerged.

### 3.2. $Y_5Si_3$–$Zr_5Si_3$ solid solutions

Samples were prepared not by reacting the two end member phases, because of course, as shown above, $Zr_5Si_3$ does not exist; instead, Y–Zr–Si pieces were melted in the appropriate atomic proportions. The results are summarized in Table 2 and Fig. 2, but the following comments highlight some of the trends in behaviour. First, a hexagonal $D8_8$ phase with decreasing unit cell volume is the main product in the unannealed material. All methods of examination show that not until $Z_{4.0}Zr_{1.0}Si_3$ is reached is there evidence for any extra phase other than residual Y–Zr–Si eutectic from the unreacted starting materials. After the $Y_{4.0}Zr_{1.0}Si_3$ composition is passed, then more eutectic and tetragonal "$Zr_2Si$"-like material also appears.

TABLE 2. Arc-cast $Y_5Si_3$–$Zr_5Si_3$ samples

| Composition | | Lattice parameters | | Cell volume ($nm^3$) | Notes | $H_2$ parameters | | |
|---|---|---|---|---|---|---|---|---|
| Y | Zr | *a* (nm) | *c* (nm) | | | Reaction start (°C) | Desorb temp. (°C) | H ($mol^{-1}$) |
| 5 | 0 | 0.8442 | 0.6353 | 0.3921 | | 410 | 475 | 0.95 |
| 4.9 | 0.1 | 0.8412 | 0.6350 | 0.3891 | | 350 | 450 | 0.65 |
| 4.8 | 0.2 | 0.8413 | 0.6307 | 0.3866 | | 350 | 440 | 0.71 |
| 4.75 | 0.25 | 0.8412 | 0.6292 | 0.3856 | | 360 | 435 | 0.70 |
| 4.65 | 0.35 | 0.8398 | 0.6303 | 0.3850 | | | 434 | 0.80 |
| 4.68 | 0.32 | 0.8399 | 0.6278 | 0.3835 | | | | |
| 4.50 | 0.50 | 0.8384 | 0.6264 | 0.3813 | | 320 | 410 | 0.55 |
| 4.25 | 0.75 | 0.8370 | 0.6224 | 0.3776 | Y–Zr–Si eutectic + $Zr_{3.3}Y_{1.8}Si_3$ | 270 | 350<br>400 | 0.80<br>0.80 |
| 4.21 | 0.79 | $(1.456_5)_{ss}$ | 0.6266 | | Ge = 0.64 supercell $a = 3\sqrt{a_{ss}}$ | 266 | 316<br>375 | 0.40<br>0.80 |
| 4.1 | 0.9 | 0.8341 | 0.6193 | 0.3731 | X-ray lines very broad | | | |
| 4.0 | 1.0 | 0.8347 | 0.6289 | 0.3795 | "$Zr_2Si$" + Y | | | |
| 3.8 | 1.2 | 0.9327 | 0.6157 | 0.3697 | $Zr_{3.4}Y_{1.76}Si_3$ | | | |
| 3.6 | 1.4[a] | 0.8297 | 0.5902 | 0.3519 | "$Zr_2Si$" present | | | |
| 3.4 | 1.6 | 0.8075 | 0.5722 | 0.3231 | "$Zr_2Si$ + eutectic | $D8_8$ phase no reaction with $H_2$ | | |
| 0.9 | 4.1 | 0.8042 | 0.5671 | 0.3176 | Eutectic | No reaction except with eutectic: $YH_3$, $ZrH_2$ | | |
| 0.5 | 4.5 | 0.8000 | 0.5597 | 0.3102 | Main phase $Zr_{4.55}Y_{0.45}Si_3$ plus $Zr_2Si$ | | | |
| 0.3 | 4.7 | 0.7993 | 0.5598 | 0.3097 | "$Zr_2Si$" | Only slight $H_2$ reaction | | |
| 0 | 5.0 | 0.7959 | 0.5561 | 0.3050 | 10% Zr + $Zr_5Si_4$ | | | |

[a]Includes scandium as well as zirconium.

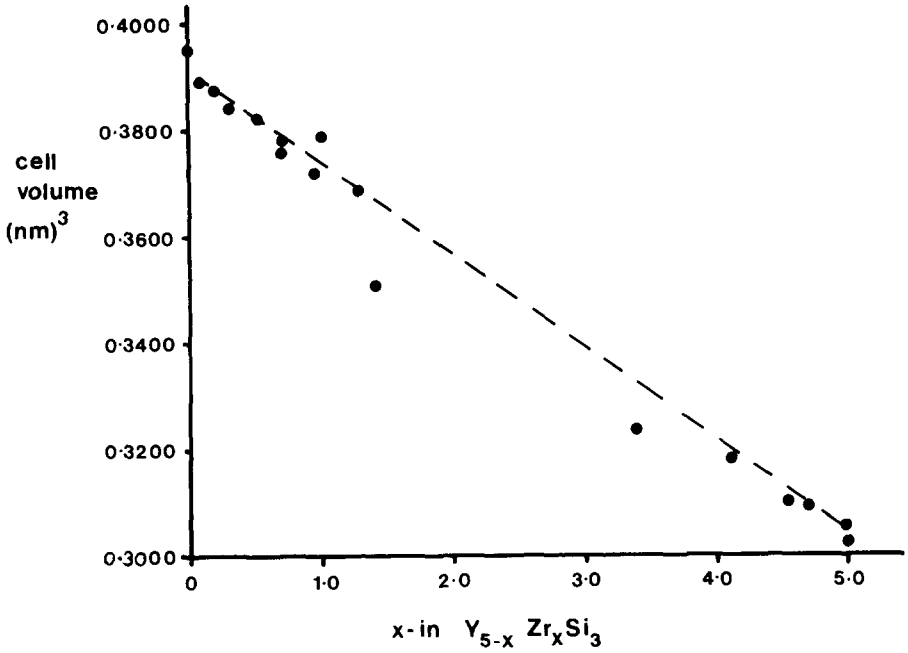


Fig. 2. Plot of unit cell volume for metastable $Y_{5-x}Zr_xSi_3$ $D8_8$ phases against composition.

The first preparation with significant amounts of unreacted Y–Zr–Si eutectic is the $Y_{4.25}Zr_{0.75}Si_3$ sample, as Fig. 3 shows. The EDX analysis across the grains is summarized in the figure caption and suggests a slight coring effect as zirconium concentrates near a grain edge. From these data we can see that the $D8_8$ phase in fact contains about 33% less zirconium than the starting composition indicates. Table 2 shows the effect the two-phase mixture has on the hydrogen reactivity with two desorption plateaux, one corresponding to the $YH_3 \rightarrow YH_2$ transformation occurring at 400 °C and accounting for 0.8H mol$^{-1}$ and the other corresponding to the 350 °C desorption of 0.4H mol$^{-1}$ coming from the $D8_8$ silicide. The total of 1.20H mol$^{-1}$ makes this an interesting sample for hydrogen storage or hydrogen control where substantial waste heat is available. In this respect it is also worth drawing attention to the $Y_{4.21}Zr_{0.79}Si_{2.36}Ge_{0.64}$ sample which forms a hydride also showing two desorption plateaux, but this time containing no significant amounts of Y–Zr–Si eutectic. In fact the preparation is virtually single phased, with only a trace (less than 2%) of a "$Zr_2Si$" phase. The significant difference here is that the 5:3 phase shows a clear superlattice pattern of the $\beta$-type silicide. In an earlier paper [3] on the Y–Ge–Si system other ordered superstructure phases in the $MSi_1Ge_2$ region were found and these too had multiplateaux desorptions at lower than expected temperatures. Here we see this pattern repeated with a low temperature desorption at 316 °C of 0.4H mol$^{-1}$ and a somewhat higher desorption at 375 °C of 0.8H mol$^{-1}$. The cycling stability of this material was noted and the suggestion that supercell silicide–germanide phases may be useful hydrogen storage media should be followed up. The inclusion of an even poorer hydride former than silicon, namely germanium, in the non-metal lattice continues to decrease the overall hydride stability as might be expected.

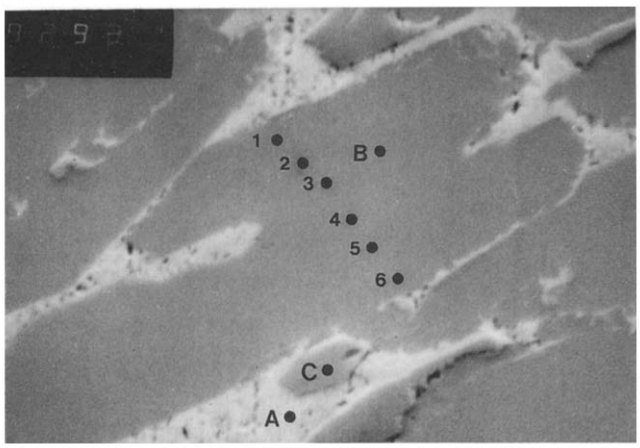


Fig. 3. Scanning electron micrograph of arc-cast $Y_{4.25}Zr_{0.75}Si_3$ sample. Area denoted by A is a eutectic of starting materials, Y:Zr:Si = 6.6:1:1. Area B is a cored $Y_{4.5}Zr_{0.5}Si_3$ region. The spot analyses are (1) $Y_{4.47}Zr_{0.60}Si_3$, (2) $Y_{4.47}Zr_{0.54}Si_3$, (3) $Y_{4.47}Zr_{0.60}Si_3$, (4) $Y_{4.47}Zr_{0.56}Si_3$, (5) $Y_{4.50}Zr_{0.53}Si_3$ and (6) $Y_{4.55}Zr_{0.51}Si_3$.

For some samples the hydride X-ray lattice parameters have been determined and can be compared with those of the starting material. They all show a common feature of a decrease in *a* axis parameter accompanied by an increase in *c* axis length, but the overall effect is only a small increase in cell volume which would minimize decrepitation problems; this information is

TABLE 3. Change in X-ray parameters of some hydrided phases

| Phase | Alloy parameters | | Cell volume ($nm^3$) | Hydride parameters | | Cell volume ($nm^3$) |
|---|---|---|---|---|---|---|
| | $a$ (nm) | $c$ (nm) | | $a$ (nm) | $c$ (nm) | |
| $Y_{4.65}Zr_{0.35}Si_3$ (annealed) | 0.8395 | 0.6307 | 0.3852 | 0.8368 | 0.6491 | 0.3936 |
| $Y_{4.68}Zr_{0.32}Si_3$ | 0.8399 | 0.6274 | 0.3835 | 0.8380 | 0.6289 | 0.3825 |
| $Y_{4.25}Zr_{0.75}Si_3$ (arc cast) | 0.8370 | 0.6224 | 0.3776 | 0.8342 | 0.6418 | 0.3868 |
| $Y_{4.0}Zr_{1.0}Si_3$ (arc cast) | 0.8347 | 0.6289 | 0.3795 | 0.8336 | 0.6464 | 0.3890 |
| $Y_{0.9}Zr_{4.1}Si_3$ (arc cast) | 0.8042 | 0.5671 | 0.3176 | 0.8064 | 0.5669 | 0.3192 |
| $Y_{1.6}Zr_{3.4}Si_3$ | 0.8075 | 0.5722 | 0.3231 | 0.8090 | 0.5722 | 0.3243 |

collected in Table 3, which also shows the very small reactivity the zirconium-rich phases $Zr_{4.1}Y_{0.9}Si_3$ and $Zr_{3.4}Y_{1.6}Si_3$ have for hydrogen under the conditions used here.

To demonstrate the metastable nature of these solid solutions and to probe the limiting compositions, some of the preparations were annealed at 1250 °C for 7 days and the samples re-examined. A summary of the results is contained in Table 4. In general the annealing produces limiting $Y_{5-x}Zr_xSi_3$ $D8_8$ phase and a tetragonal phase plus a small amount of yttrium metal. The average composition from the EDX analysis for the $D8_8$ phase was $Y_{4.74}Zr_{0.27}Si_3$, while the X-ray analysis, based on calculating the unit cell volume from the lattice parameters, gives a limiting composition of $Y_{4.81}Zr_{0.19}Si_3$, and so it is reasonable to quote the composition of the ternary phase to be $Y_{4.78}Zr_{0.23}Si_3$. In support of this it is noteworthy that the $Y_{4.65}Zr_{0.35}Si_3$ preparation contains a $D8_8$ phase analysing to $Y_{4.75}Zr_{0.23}Si_3$ which has X-ray parameters $a=0.8398$ nm and $c=0.6303$ nm, and after the 7 day anneal at 1050 °C still contains a $D8_8$ phase with essentially identical parameters $a=0.8398$ nm and $c=0.6307$ nm. In this sample the tetragonal phase has a composition unusually rich in yttrium: $Y_{1.01}Zr_{0.8}Si$. This phase produced few, very strain-broadened lines such that lattice parameter values could not be found with real confidence. In general the annealed samples were treated at 1250 °C and the tetragonal phase was found to have a composition in the range $Zr_{1.83-1.95}Y_{0.06-0.21}Si$ depending on the starting yttrium content. These figures suggest that the phase is yttrium-substituted $Zr_2Si$ and that this phase has a limiting composition around $M_2Si$ and not the $M_4Si$ previously reported for this phase. Since there is no $Y_2Si$ phase, the possible existence of $YZr_{0.8}Si$ at 1050 °C is of some interest. All the tetragonal metal-rich silicides are essentially inert to hydrogen gas at temperatures up to 700 °C at 1 atm pressure.

Where the yttrium metal was clearly identified in the X-ray pattern, the lattice parameters were smaller than those for pure yttrium, $a=0.36474$ nm and $c=0.57306$ nm, as the results in Table 4 demonstrate. This suggests that the metal phase contains some zirconium.

At the $Zr_{5-x}Y_xSi_3$ end of the series the collected data suggest that $x$ must exceed 0.45 before a stable $D8_8$ phase can occur after annealing at 1250 °C.

In order to clarify these findings, several metal-rich compositions were arc melted, phase analysed, hydrogen tested and then annealed at 1250 °C and re-examined. Some of the data from these tests are presented in Table 4, while Fig. 4 presents a 1250 °C section of the ternary Y–Zr–Si diagram constructed to accommodate the new information of the phases found in the X-ray patterns and their compositions from the SEM analyses. In Fig. 4 the letters correspond to the samples so labelled in Table 5.

## 4. Summary

Fast cooling on the hearth or an argon arc furnace leads to metastable $D8_8$ solid solutions between $Y_5Si_3$, a stable precursor, and $Zr_5Si_3$, an unstable precursor. These metastable $Y_{5-x}Zr_xSi_3$ phases occur despite the substantial unit cell volume difference between the end members of some 22%. Beyond the composition $Y_{4.25}Zr_{0.75}Si_3$ each preparation has up to 20% of starting element eutectic plus yttrium-substituted $Zr_2Si$ hemisilicide. The high percentage of $D8_8$ material has enabled a hydrogen reactivity investigation to be made which demonstrates clearly that the presence of zirconium in the structure partially destabilizes hydrides that are formed, enabling 0.55–0.95H $mol^{-1}$ to be desorbed rapidly. Fast hydrogen evolution of this type occurs at 350 °C in $Y_{4.25}Zr_{0.75}Si_3$ compared with 475 °C in $Y_5Si_3$. However, the amount of hydrogen undergo-

TABLE 4. Effect of annealing at 1250 °C on Y–Zr–Si preparations

| Composition | Cast | | | Annealed | | |
|---|---|---|---|---|---|---|
| | Phases | Lattice parameters (nm) | | Phases | Lattice parameters (nm) | |
| $Y_5Si_3$ | Hexagonal | 0.8442 | 0.6363 | Hexagonal | 0.8442 | 0.6353 |
| $Y_{4.65}Zr_{0.35}Si_3$ | Mixture Y:Zr:Si = 6.5:1.06:1.0 | | | Small amount tetragonal | | |
| | + | | | $Zr_{0.8}Y_{1.02}Si$ | 0.664 | 0.517 |
| | $Y_{4.75}Zr_{0.23}Si_3$ | | | $Y_{4.71}Zr_{0.22}Si_3$ | 0.8398 | 0.6307 |
| | Hexagonal | 0.8398 | 0.6303 | | | |
| $Y_{4.25}Zr_{0.75}Si_3$ | Y:Zr:Si (eutectic) = 6.5:1.04:1.0 | $0.363_1$ | $0.570_9$ | Small amount tetragonal $Zr_{1.83}Y_{0.21}Si$ | 0.664 | 0.517 |
| | Hexagonal $Y_{4.49}Zr_{0.55}Si_3$ | 0.8370 | 0.6224 | Hexagonal $Y_{4.8}Zr_{0.3}Si$ | 0.8419 | 0.6348 |
| $Y_{4.0}Zr_{1.0}Si_3$ | Y–Zr | $0.363_4$ | 0.5667 | Y metal | | |
| | Tetragonal | $0.660_5$ | 0.5158 | + | | |
| | | | | tetragonal $Zr_{1.95}Y_{0.12}Si$ | $0.661_5$ | $0.528_7$ |
| | Hexagonal | 0.8347 | 0.6289 | + | | |
| | | | | hexagonal $Y_{4.92}Zr_{0.19}Si_3$ | 0.8403 | 0.6320 |
| $Zr_5Si_3$ | Hexagonal $D8_8$ | 0.7959 | 0.5561 | *No* hexagonal | | |
| | | | | Orthorhombic ZrSi | 0.7033 | 0.3750, 0.5305 |
| | + | | | + | | |
| | $Zr_5Si_4$ | Too weak to find | | "$Zr_2Si$" | $0.668_4$ | $0.515_2$ |
| | + | | | | | |
| | ZrSi | | | | | |
| $Zr_5Ge_3$ | $Zr_{5.4}Ge_4$ | Orthorhombic | | $D8_8$ hexagonal $Zr_5Ge_3$ | 0.8053 | 0.5620 |
| | + | | | | | |
| | $Zr_{2.9}Ge$ | Tetragonal | | | | |
| $Y_{4.5}Zr_{4.5}Si_3$ | $Zr_{4.1}Y_{1.1}Si_3$ | 0.8042 | 0.5671 | Hexagonal $Y_{4.6}Zr_{0.23}Si_3$ | 0.8414 | 0.6318 |
| | | | | + | | |
| | | | | tetragonal $Zr_{1.87}Y_{0.1}Si$ | 0.6613 | 0.5300 |
| | | | | + | | |
| | | | | Y | 0.3642 | 0.5734 |

*(continued)*

TABLE 4. (*continued*)

| Composition | Cast | | | Annealed | | |
|---|---|---|---|---|---|---|
| | Phases | Lattice parameters (nm) | | Phases | Lattice parameters (nm) | |
| $Y_{3.0}Zr_{3.0}Si_{3.0}$ | Hexagonal $Y_{4.68}Zr_{0.42}Si_3$ + hexagonal $Zr_{3.59}Y_{1.55}Si_3$ + tetragonal $Y_{1.64}Zr_{0.16}Si$ + Y:Zr:Si = 7:1:1 | 0.8380<br>0.8075<br>0.6605<br>0.3646 | 0.6289<br>0.5722<br>0.5283<br>0.5726 | Hexagonal $Y_{4.71}Zr_{0.23}Si_3$ + tetragonal $Y_{1.92}Zr_{0.06}Si$ + Y | 0.8396<br>0.6602 | 0.6307<br>0.5299 |
| $Y_{0.6}Zr_{5.4}Si_3$ | Hexagonal $Zr_{4.86}Y_{0.3}Si_3$ + tetragonal $Zr_{1.99}Y_{0.08}Si$ + Zr:Y:Si = 2:4:1 | 0.7993<br>0.6611 | 0.5598<br>0.5305 | Hexagonal $Zr_{4.0}Y_{1.3}Si_3$ + tetragonal $Zr_{1.87}Y_{0.1}Si$ | 0.7998<br>0.6612 | 0.5593<br>0.5307 |
| $Y_{0.6}Zr_{9.9}Si_3$ | Zr–Y + $Zr_{1.99}Y_{0.6}Si$ | | | Hexagonal Zr + tetragonal $Y_{1.99}Zr_{0.22}Si$ + alloy | | |

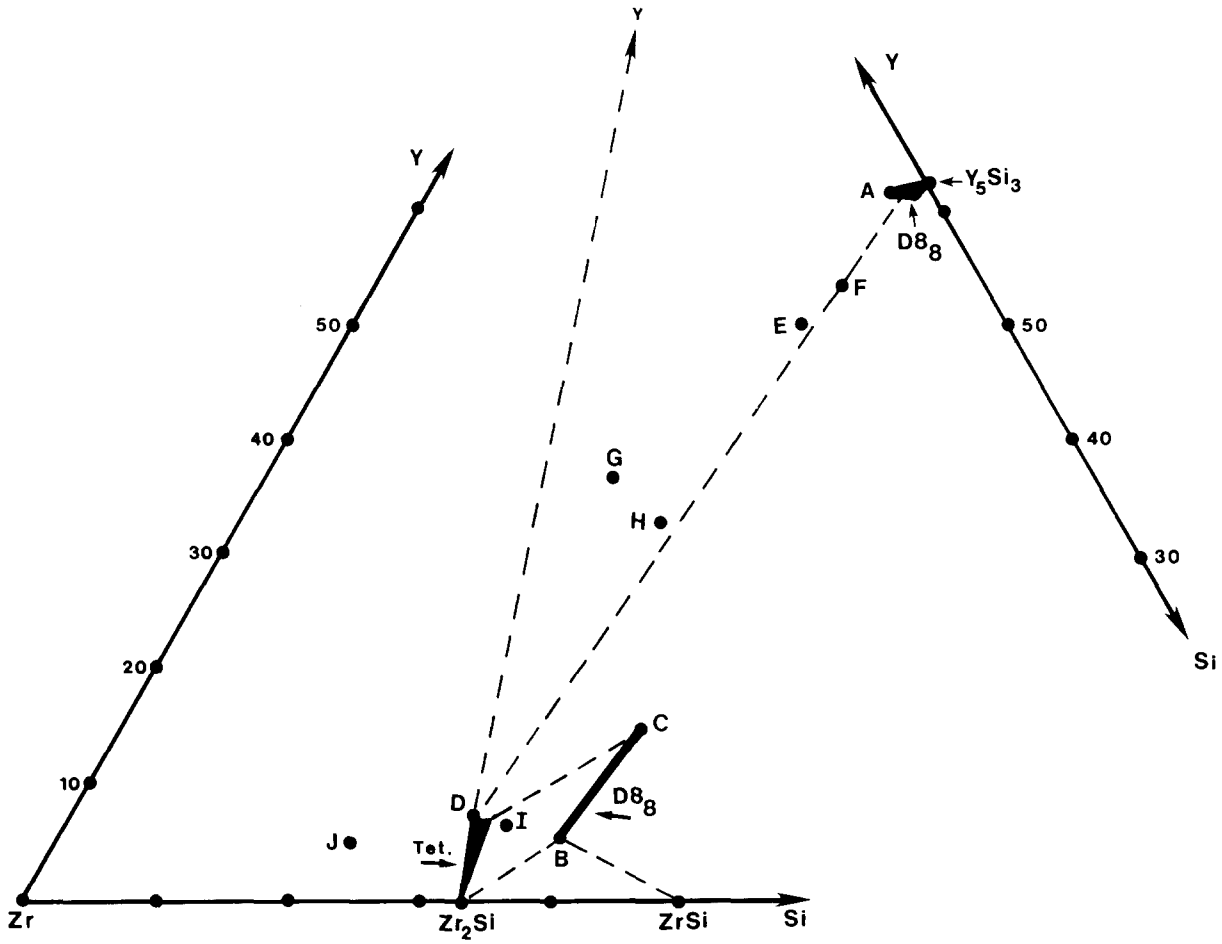


Fig. 4. A section of the Y–Zr–Si diagram at 1250 °C. The letters A, B, etc. are samples examined and the phase analysis for these points is given in Table 5.

TABLE 5. Phases found for the points marked on Fig. 4

| Sample | Overall composition | Phases present in X-ray pattern and SEM analysis |
|---|---|---|
| A | $Y_{4.78}Zr_{0.23}Si_3$ | Limit of $D8_8$ solid solution |
| B | $Zr_{4.55}Y_{0.45}Si_3$ | Limit of zirconium-rich $D8_8$ phase |
| C | $Zr_{4.0}Y_{1.1}Si_3$ | Upper limit of yttrium in $D8_8$ |
| D | $Zr_{1.83}Y_{0.21}Si_3$ | Maximum Y–Zr content tetragonal hemisilicide phase |
| E | $Y_4Zr_1Si_3$ | $Y_{4.92}Zr_{0.19}Si_3$ + Y metal + $Zr_{1.95}Y_{0.12}Si$ |
| F | $Y_{4.23}Zr_{0.75}Si_3$ | $Y_{4.8}Zr_{0.3}Si_3 + Zr_{1.83}Y_{0.21}Si$ |
| G | $Y_{4.5}Zr_{4.5}Si_3$ | $Y_{4.6}Zr_{0.23}Si_3$ + Y metal + $Ze_{1.87}Y_{0.1}Si$ |
| H | $Y_3Zr_3Si_3$ | $Y_{4.71}Zr_{0.23}Si_3 + Zr_{1.92}Y_{0.06}Si$ + Y metal |
| I | $Y_{0.6}Zr_{5.4}Si_3$ | $Zr_{4.0}Y_{1.3}Si_3 + Zr_{1.87}Y_{0.1}Si$ |
| J | $Y_{0.6}Zr_{9.9}Si_3$ | Zr metal + $Zr_{1.99}Y_{0.06}Si$ + alloy |

ing this absorption and desorption decreases from 0.95H mol$^{-1}$ in $Y_5Si_3$ to 0.35H mol$^{-1}$ in the solid solution phase.

All other solid solutions containing more than 0.75Zr mol$^{-1}$ react only slowly with hydrogen, producing a stable hydride that adjusts its composition slowly when heated and cooled in 1 atm $H_2$; for example, $Zr_5Si_3$ absorbs up to a composition $Zr_5Si_3H_{1.48}$ and then over a 575 °C temperature interval desorbs slowly to a $Zr_5Si_3H_{1.0}$ composition. The yttrium eutectic present in these quenched melts reacts rapidly at unexpectedly low temperatures with hydrogen, while the tetragonal hemisilicide is essentially inert to hydrogen under the conditions applying to this investigation.

One sample containing some germanium substituted for silicon, and examined to see if the fast-reversing hydride phase could be preserved to higher zirconium contents, has resulted in an essentially $D8_8$ phase, but in this case a superstructure variant, which reversibly absorbs and desorbs 1.2H mol$^{-1}$ in two temperature regimes below a maximum of 380 °C. This improved behaviour is worthy of further detailed investigation, especially since it seems to be associated with the extended *a* parameter supercell structure. A similar composition $MSi_{2.46}Ge_{0.64}$ has been shown previously

to have the supercell [3] and to produce a similar effect.

Unlike $Zr_5Si_3$ which occurred on rapid cooling but which was not stable at 1250 °C, giving way to $Zr_2Si$ and ZrSi, the germanide $Zr_5Ge_3$ could only be made by annealing the arc-melted mixture. The quenched mixture was not reactive to hydrogen and the $D8_8$ $Zr_5Ge_3$ has not so far been tested.

All the metastable preparations decomposed on annealing at 1250 °C for 7 days into mixtures of the limiting compositions $Y_{4.78}Zr_{0.23}Si_3$, $Zr_{4.55}Y_{0.45}Si_3$, $Zr_{4.0}Y_{1.1}Si$, $Zr_{1.83}Y_{0.21}Si$ and yttrium or zirconium metal, and these phases have been shown to occur when various metal-rich silicon mixtures are first arc melted and then annealed. There is a suggestion that a lower annealing temperature, 1050 °C, can lead to a hemisilicide containing almost equal atomic amounts of yttrium and zirconium, $Y_{1.02}Zr_{0.8}Si$, even though a corresponding phase does not occur in the Y–Si binary system. A section of the Y–Zr–Si diagram at 1250 °C has been constructed.

## Acknowledgments

J.M.W. was in receipt of a SERC studentship during the time part of this work was done. I.J.M. is pleased to acknowledge receipt of a Flinders University Visiting Senior Fellowship during the time the data were prepared for publication and the manuscript was written.

## References

1 I. J. McColm, V. Kotroczo, T. W. Button, N. J. Clark and B. Bruer, *J. Less-Common Met., 115* (1986) 113–125.
2 I. J. McColm and V. Kotroczo, *J. Less-Common Met., 131* (1987) 191–199.
3 I. J. McColm and J. M. Ward, *J. Alloys Comp., 178* (1992) 91.
4 R. C. Weast (ed.), *CRC Handbook of Chemistry and Physics,* CRC Press, London, 66th edn., 1985.
5 J. F. Stampfer, *Chem. Abstr., 65* (1966) 19354.
6 V. Kotroczo, I. J. McColm and J. N. Clark, *J. Less-Common Met., 132* (1987) 1–13.
7 O. Schob, H. Nowotny and F. Benesovsky, *Monatsh. Chem., 92* (1961) 1218.
8 T. W. Button, I. J. McColm and J. M. Ward, *J. Less-Common Met., 159* (1990) 205–222.
9 L. Brewer and O. Krikorian, *J. Electrochem. Soc., 103* (1956) 38.
10 C. E. Lundin, D. J. McPherson and M. Hansen, *Trans. Am. Soc. Met., 45* (1953) 901.
11 M. Massalski, *Binary Alloy Phase Diagrams,* American Society for Metals, Materials Park, OH, 1990.